Reconsideration of the relaxational and vibrational line shapes of liquid water based on ultrabroadband dielectric spectroscopy

Journal:	*Physical Chemistry Chemical Physics*
Manuscript ID	CP-ART-07-2018-004778.R1
Article Type:	Paper
Date Submitted by the Author:	05-Oct-2018
Complete List of Authors:	Shiraga, Keiichiro; RIKEN, Integrative Medical Sciences t, k; Kyoto University Arikawa, Takashi; Kyoto University Saito, Shinji; Institute for Molecular Science, Theory and Computational Molecular Science Ogawa, Yuichi; Kyoto University,

Reconsideration of the relaxational and vibrational line shapes of liquid water based on ultrabroadband dielectric spectroscopy

Keiichiro Shiraga[*a] keiichiro.shiraga@riken.jp

Koichiro Tanaka[bc] kochan@scphys.kyoto-u.ac.jp

Takashi Arikawa[b] arikawa@scphys.kyoto-u.ac.jp

Shinji Saito[de] shinji@ims.ac.jp

Yuichi Ogawa[f] ogawayu@kais.kyoto-u.ac.jp

[a] RIKEN Center for Integrative Medical Sciences, Suehiro-cho, Tsurumi-ku, Yokohama, Kanagawa 230-0045, Japan

[b] Department of Physics, Graduate School of Science, Kyoto University, Kitashirakawa-oiwakecho, Sakyo-ku, Kyoto 606-8502, Japan

[c] Institute for Integrated Cell-Material Sciences (iCeMS), Kyoto University, Sakyo-ku, Kyoto 606-8501, Japan

[d] Department of Theoretical and Computational Molecular Science, Institute for Molecular Science, Myodaiji, Okazaki, Aichi 444-8585, Japan

[e] The Graduate University for Advanced Studies, Myodaiji, Okazaki, Aichi 444-8585, Japan

[f] Graduate School of Agriculture, Kyoto University, Kitashirakawa-oiwakecho, Sakyo-ku, Kyoto 606-8502, Japan

* Corresponding author E-mail. keiichiro.shiraga@riken.jp

Footnotes Electronic Supplementary Information (ESI) available.

Abstract

The Debye relaxation function is widely used to describe the large dielectric dispersion of ambient water around 20 GHz. However, from a theoretical point of view, this function is supposed to give incorrect predictions at high frequencies owing to the inappropriate assumption that inertial effects and intermolecular interactions do not affect the relaxation dynamics. Our ultrabroadband spectroscopy of liquid water ranging from 500 MHz to 400 THz did demonstrate that the Debye is inaccurate far above the microwave region. As an alternative, we tried a stochastic frequency modulation (SFM) model assuming instantaneous modification of the line shapes by the with the surrounding system. The SFM relaxation model reproduced the experimental dielectric spectra up to 400 THz, showing that the hydrogen-bond dynamics are associated with the inertial effect that causes the non-exponential relaxation behaviour in a very short time (typically 25 fs). Within the framework of this relaxation model, the hindered translation modes are able to be approximated as fast modulation (homogeneous) line shapes because the interaction time with frequency modulation is too short. Compared with them, the libation mode is found to have a relatively slow modulation (inhomogeneous) origin, where disturbance of water hydrogen bonds induced by the hindered translations leads to fluctuations in the libration frequency.

1. Introduction

Liquid water has an extremely large static permittivity ($\varepsilon_S \approx 80$ at room temperature) compared with other polar liquids, primarily because of the intense relaxation mode centred at about 20 GHz in the complex dielectric constant $\tilde{\varepsilon}(\omega)$.[1,2] Despite the dynamically heterogeneous hydrogen-bond (HB) network of liquid water, this relaxation can be almost perfectly described by the Debye relaxation model, which is reduced to a single exponential decay in the auto-correlation function. A recent theoretical study proposed that the single exponential decay of water relaxation originates from significant dipole correlations (i.e. long-range HB dynamics) on scales of 1.5-2.0 nm.[3] On the other hand, $\tilde{\varepsilon}(\omega)$ of ambient water starts to deviate from the single Debye function in the higher microwave region,[2] and this deviation has been historically made up for by adding secondary[2,4-6] and tertiary[7] Debye components whose origin are structurally[4,5] or dynamically[6] different from the main relaxation at around 20 GHz. More recently, Popov *et al.* developed a new relaxation model, called defect-migration theory,[8] which assumes that the main Debye relaxation of liquid water is driven by migration of defects through the HB network, like Bjerrum defects in ice.[9] Within this scope, the additional Debye components are not required, because the defect migration causes vibrations in the HB network and gives rise to a larger response above the relaxation frequency. Although the consensus is yet to be reached about water relaxation, the Debye model and its derivatives are very widely believed to *phenomenologically* explain the dielectric dispersion around 20 GHz.

Nevertheless, it should be kept in mind that the Debye relaxation is *theoretically* grounded in the diffusion limit, where extremely complex dipolar relaxations at long times can be treated statistically, neglecting the moment of inertia of the dipoles and intermolecular interactions. However, for highly anisotropic and strongly dipolar molecules such as water, their effects should be rigorously taken into account at such short times that an equilibrium statistical description is inapplicable.[10-12] Indeed, the imaginary part of the Debye model whose high-frequency tail decays as ω^{-1} results in a constant absorption, $\alpha(\omega) \propto \omega \mathrm{Im}[\tilde{\varepsilon}(\omega)]$, above the THz region, but this background absorption, typically $\alpha \approx 150$ cm^{-1} at room temperature,[13] occasionally exceeds the actual absorption of water in 75~80 THz ($\alpha \approx 120$ cm^{-1}) and above 120 THz ($\alpha \ll 100$ cm^{-1}).[14,15] This inconsistency is the consequence of the theoretical inaccuracy of the Debye model far above the microwave region and calls for an alternative relaxation model that considers the effects of inertia and the intermolecular interactions in order to describe the high-frequency tail of the relaxation line shape. The stochastic frequency modulation (SFM) model,[16] which was proposed by Shibata *et al.* on the basis of Kubo's line shape theory,[17] is a solvable model that meets the above requirements: it deals with the inertial effect and intermolecular interactions as a correlation with the thermal bath, allowing observation of the relaxation behaviour from the short to long times in a practical way. Applying the SFM model to the Raman-active susceptibility spectra of water showed that neglect of these effects is anything but acceptable.[18] Hence, we come to the conclusion that the validity of the Debye model must be recon-

sidered for the dipolar relaxations as well: yet this issue has so far remained unaddressed.

It is known that the hindered translational and rotational intermolecular modes of water are spread over a 1~20 THz range and their band shapes reflect the dynamical structure of water.[19-23] However, these bands unexceptionally overlap with neighbouring vibration and relaxation modes,[5,24] complicating the characterisation of their band shapes behind a broad spectrum without a fitting procedure. In this circumstance, the relaxation model must be optimized to determine the true band shapes of the intermolecular vibration modes because there is every possibility that the Debye model is inaccurate in the THz region.

In this study, an ultrabroadband complex dielectric spectrum of liquid water, ranging from 500 MHz to 400 THz, was collected to resolve the issue of the Debye model. On the basis of the optimised relaxation model taking SFM processes into consideration, the intermolecular vibrations of water were re-examined so as to characterise their true line shapes.

2. Experimental

Normal water, H_2O, demineralized to >3 MΩ·cm and deuterium water, D_2O, (99.9 % purity, Wako Pure Chemical Industries, Ltd.) were used as samples without further purification.

Ultrabroadband dielectric spectra, where the real $\mathrm{Re}[\tilde{\varepsilon}]$ and imaginary $\mathrm{Im}[\tilde{\varepsilon}]$ parts project the in-phase and out-of-phase polarization components, of liquid H_2O and D_2O at 300 K were obtained over a range of 500 MHz and 400 THz (0.017~13333 cm^{-1} in wavenumber and 600 mm~750 nm in

wavelength), by using seven spectroscopic systems: a vector network analyser (VNA, 500 MHz~50 GHz), low-frequency terahertz time-domain attenuated total reflection spectroscopy (THz TD-ATR, 50 GHz~1 THz), high-frequency THz TD-ATR spectroscopy (1~4 THz), far-infrared Fourier-transform attenuated total reflection spectroscopy (FIR FT-ATR, 4~15 THz), mid-infrared Fourier-transform spectroscopy (MIR FTS, 15~23 THz), mid-infrared Fourier-transform attenuated total reflection spectroscopy (MIR FT-ATR, 23~120 THz) and near-infrared spectroscopy (NIR spectroscopy, 120~400 THz).

A VNA (N5247A, Agilent, Ltd.) in combination with an open-ended coaxial probe 85070E (Agilent, Ltd.) was used for the measurements between 500 MHz and 50 GHz. The scattering parameters were recorded by immersing the probe in the sample after the calibration with three different loads (air, short-circuit, and ultrapure water), and then the complex dielectric constant was derived. In turn, two THz TD-ATR spectroscopic systems equipped with a Dove-type ATR prism[25] (incident angle of 51.6°) made of a >20 kΩ·cm silicon measured the complex dielectric constants from 50 GHz to 4 THz. Low-frequency THz TD-ATR measurements were made using a spectroscopy platform TAS7500TS (Advantest Corp.) adopting the asynchronous optical sampling technique. Femtosecond laser pulses (λ=1.55 μm in wavelength: ≤50 fs duration) were focused onto a biased bowtie photoconductive (PC) antenna for it to emit THz pulses. They were then led to the ATR prism, and the reflected THz pulses were eventually detected by a dipole PC antenna. After the re-

flectance and phase shift spectra were calculated by taking the Fourier transform of the THz time-domain waveforms, the complex dielectric constant was derived according to Fresnel's formula. Another THz TD-ATR system was used in the higher frequency region up to 4 THz: it consists of a mode-locked Ti:sapphire laser (Femtolasers, Ltd.) with a centre wavelength of λ=800 nm and a pulse duration of 10 fs as an excitation source, [110]-oriented GaP with a thickness of 300 μm as an emitter, and a bowtie PC antenna as a detector.[26] The FIR FT-ATR measurements covering 4~15 THz were carried out with a FARIS-1s spectrometer (Jasco Corp.). A ceramic heater and deuterated triglycine sulfate were used as a light source and detector, respectively, and a silicon ATR prism was placed at the focal position of the light path at an incident angle of 45°. The measured polarized reflectance spectrum was subjected to a Kramers-Kronig transform[27] to calculate the phase shift spectra. The details and validity of the Kramers-Kronig transformation are referred elswhere.[26,28] MIR spectra over 15 and 120 THz were collected using an FT-IR spectrometer (FT/IR-4600, Jasco Corp.). The lower frequency part (15-23 THz) was measured with a transmission cell consisting of two 300-μm-thick Si windows separated by a steel spacer with 10 μm thickness. The obtained absorbance spectrum was firstly transformed into the extinction coefficient $\kappa(\omega)$ based on the Lambert-Beer law, and $\kappa(\omega)$ was then subjected to the Kramers-Kronig relation to derive the refractive index $n(\omega)$.[29] Next, the complex dielectric constant in this region was derived using the relationship: $\tilde{\varepsilon}(\omega) = \big(n(\omega) - i\kappa(\omega)\big)^2$. On the other hand, the high-frequency part (23-120 THz) was

measured in the ATR geometry, where an ATR prism made of diamond was used. The derivation process of the complex dielectric constant was identical with that of the FIR FT-ATR mentioned above. Lastly, the highest frequencies up to 400 THz were collected by a V-670 UV-VIS-NIR spectrophotometer (Jasco Corp.) with a transmission scheme. A combination of three quartz cells with different sample thicknesses (0.1 mm, 1 mm and 10 mm) allowed us to obtain complete absorption spectra. Similar to the case of the MIR FTS, the absorbance spectra were subjected to the Kramers-Kronig transformation to determine the complex dielectric constant.[29]

More than five replicate samples were measured to confirm the reliability in each system. The error ratio (i.e. the experimental uncertainty to the average) for the real and imaginary part for H_2O was less than 1.5 % and 1.6 %, respectively, in the entire measured region.

3. Results & Discussion

Conventional fitting with the Debye-DHO model. Fig. 1 shows the obtained ultrabroadband complex dielectric constant $\tilde{\varepsilon}(\omega)$ and absorption coefficient $\alpha(\omega)$ of liquid H_2O and D_2O at 300 K. The frequency dispersion of the intense relaxation (GHz region), the intermolecular vibrations (THz region), and the intramolecular bands (IR region) is almost perfectly consistent with the "patched" broadband spectra estimated from a number of previous reports independently published by different groups.[1,2,5,14,15,30,31] We emphasise here that our ultrabroadband spectra, completely covering from the microwave to NIR, measured from the same water sample at the same tempera-

ture stands out as having been measured by a single workgroup: it is not a set of various measurements collected from different literatures.

The intense relaxation peak located around 20 GHz for H_2O involves a collective dipolar reorientation process of hydrogen-bonded water[3,32-34] (hereafter we call this mode a "slow relaxation"). With respect to the isotopic effect, the H_2O relaxation time almost completely coincides with that of D_2O if the H_2O temperature is 7.2 K lower.[34] In contrast, the resonant peak around 5 THz, which is assigned to the intermolecular stretching mode,[35-37] showed little isotope effect. The small H/D isotope effect of this mode can be understood as oxygen atoms acting as the main vibrators.[20,38] The comparative study of low-frequency Raman and dielectric spectroscopy by Fukasawa *et al.* indicates that two more modes exist between the slow relaxation and the intermolecular stretching: a weak relaxation in the sub-THz region (termed "fast relaxation", as a counterpart of the slow relaxation) and an intermolecular bending mode around 1.5 THz.[24] The intermolecular bending and stretching vibrations are collectively referred to as the hindered translation mode: they are oscillations around the instantaneous centre of mass driven by the induced dipoles.[39] In general, the intermolecular bending and stretching are assigned to the translations that are respectively transverse and longitudinal to the HBs.[40-45] Above 10 THz, all the bands undergo redshifts by a factor of $\sim\sqrt{2}$ under H/D substitution because of the movements of hydrogen atoms.[38] The lowest frequency band can be assigned to the libration ρ_L (i.e. hindered rotations governed by the permanent dipole mo-

ment),[46] and the rest are intramolecular modes such as H-O-H bending (δ_{HOH}, 49 THz) and O-H stretching (ν_{OH}, ~100 THz). In addition to the $\delta_{\mathrm{HOH}} + \rho_{\mathrm{L}}$ band (~65 THz), the overtone and combination bands above 120 THz are also recognized.

Whereas the intramolecular bands, especially the O-H stretching one, have been extensively examined using both linear and nonlinear spectroscopy so far,[47-52] the origin of the complex spectrum line shapes below the FIR region remains unclear. The most widely adopted approach to unravelling their band shapes behind a broad spectrum is a nonlinear fitting based on the Debye and damped harmonic oscillator (DHO) functions:

$$\begin{aligned}\tilde{\varepsilon}(\omega) &= \tilde{\chi}_{\mathrm{slow}}(\omega) + \tilde{\chi}_{\mathrm{fast}}(\omega) + \tilde{\chi}_{\mathrm{B}}(\omega) + \tilde{\chi}_{\mathrm{S}}(\omega) + \tilde{\chi}_{\mathrm{L1}}(\omega) + \tilde{\chi}_{\mathrm{L2}}(\omega) + \varepsilon_{\infty} \\ &= \frac{\Delta\varepsilon_{\mathrm{slow}}}{1 + i\omega\tau_{\mathrm{slow}}} + \frac{\Delta\varepsilon_{\mathrm{fast}}}{1 + i\omega\tau_{\mathrm{fast}}} + \frac{\Delta V_{\mathrm{B}}{\omega_{\mathrm{B}}}^2}{{\omega_{\mathrm{B}}}^2 - \omega^2 + i\omega\gamma_{\mathrm{B}}} + \frac{\Delta V_{\mathrm{S}}{\omega_{\mathrm{S}}}^2}{{\omega_{\mathrm{S}}}^2 - \omega^2 + i\omega\gamma_{\mathrm{S}}} \\ &\quad + \frac{\Delta V_{\mathrm{L1}}{\omega_{\mathrm{L1}}}^2}{{\omega_{\mathrm{L1}}}^2 - \omega^2 + i\omega\gamma_{\mathrm{L1}}} + \frac{\Delta V_{\mathrm{L2}}{\omega_{\mathrm{L2}}}^2}{{\omega_{\mathrm{L2}}}^2 - \omega^2 + i\omega\gamma_{\mathrm{L2}}} + \varepsilon_{\infty} \end{aligned} \quad (1)$$

$\tilde{\chi}_{\mathrm{slow}}(\omega)$ and $\tilde{\chi}_{\mathrm{fast}}(\omega)$ are the slow and fast relaxation modes described by the Debye function with the relaxation strength $\Delta\varepsilon$ and the relaxation time τ. Vibration modes such as the intermolecular bending $\tilde{\chi}_{\mathrm{B}}(\omega)$, intermolecular stretching $\tilde{\chi}_{\mathrm{S}}(\omega)$, low-frequency libration (L1) $\tilde{\chi}_{\mathrm{L1}}(\omega)$, and high-frequency libration (L2) $\tilde{\chi}_{\mathrm{L2}}(\omega)$ are represented by the DHO model with the vibration strength ΔV_{j}, resonant frequency ω_{j} and damping constant γ_{j} (the subscript j=B, S, L1 or L2). In this study, the region of interest for the fitting was limited to between 500 MHz and 23 THz, be-

cause the satellite component $\delta_{\mathrm{HOH}} - \nu_{\mathrm{L}}$ has a weak contribution above 25 THz.[47] Since the high-frequency modes including intramolecular bands and electron transitions can be regarded as a baseline of the real part, these modes can be overall treated as a high-frequency limit ε_∞. Taking the low-frequency limit $\omega \to 0$, eqn (1) gives the static permittivity: $\varepsilon_{\mathrm{S}} = \Delta\varepsilon_{\mathrm{slow}} + \Delta\varepsilon_{\mathrm{fast}} + \Delta V_{\mathrm{B}} + \Delta V_{\mathrm{S}} + \Delta V_{\mathrm{L1}} + \Delta V_{\mathrm{L2}} + \varepsilon_\infty$.

As shown in Fig. 2, eqn (1) superficially provides a good fit for liquid water at 300 K. Regarding consistency with the available previous data,[1,2,5,22,53-55] reliability of our fitting procedure gives reasonable fitted parameters of $\tilde{\chi}_{\mathrm{slow}}(\omega)$, $\tilde{\chi}_{\mathrm{fast}}(\omega)$, $\tilde{\chi}_{\mathrm{S}}(\omega)$ and ε_{S} (Table 1 and 2.) With regard to the slow relaxation mode, the Debye model well replicates the experimental $\tilde{\varepsilon}(\omega)$ in the microwave frequency range. However, it is worthy of note that at much higher frequencies, the Debye function considerably exceeds the actual imaginary part in the MIR and NIR regions (see Fig. 4). As well as the Debye model, defect-migration theory is also inconsistent with the experimental result above 60 THz. The reason is that this theory is based on a Debye function whose high-frequency tail is slightly modified by the global vibration of the HB network.[8] Concerning the libration mode, the dual-DHO function gives rise to much larger fitting residuals compared with the dual-Gaussian one in the imaginary part, suggesting that the libration mode is composed of two inhomogeneous sub-bands (see Fig. S4 of the ESI). The incompatibility of the DHO functions with the libration band is also reflected in overly large vibration strength, $\Delta V_{\mathrm{L1}} + \Delta V_{\mathrm{L2}}$ =0.83 for H_2O

and 0.93 for D_2O. These values are obviously unacceptable because the large $\Delta V_{L1} + \Delta V_{L2}$ leads to an unnaturally small ε_∞ (i.e. ε_∞ =1.75 for H_2O), which is smaller than the actual real part in the visible region ($\varepsilon_{vis} = {n_{vis}}^2 \approx 1.78$). Thus, it seems incorrect to use the DHO functions to describe the libration band of water.

In summary, the conventional Debye-DHO fitting model is insufficient in the light of the high-frequency behaviour of the Debye model and inaccurate libration band shape. In the next section, we tried to resolve these issues by demonstrating the applicability of the SFM model.

Refined fitting with the stochastic frequency modulation (SFM) model. The stochastic frequency modulation (SFM) model assumes a stochastic process in which the oscillation ω_0 is subject to frequency modulation with the amplitude of ω_Δ. Providing that the process is Markovian, the frequency fluctuation of the system given by $\omega(t) = \omega_0 + \delta\omega(t)$ undergoes an exponential time correlation characterised as $\langle \delta\omega(t)\delta\omega(0)\rangle = {\omega_\Delta}^2 \exp[-\Gamma|t|]$, where Γ is the rate of frequency modulation.[17,56] With the aid of ω_Δ and Γ, it is useful to define the modulation degree $\alpha_K = \omega_\delta/\Gamma$.[17] The negligible modulation (i.e. $\alpha_K \to 0$) is nothing but the fast modulation or motional narrowing limit whose oscillation line shape is characterised as homogeneous broadening, while the slow modulation $\alpha_K \gg 1$ yields an inhomogeneous line width.[57] Thus, the SFM model smoothly bridges the extremes of the fast to slow modulation limit. Since the fluctuation amplitude ω_Δ is associated with the moment of inertia, and the inverse modulation rate corresponds to the

characteristic time of the modulation,[58] the inertial effect and the intermolecular interactions are effectively introduced as the correlation with stochastic frequency modulation.

As a practical use for the SFM model, let us firstly consider a perturbed frequency $\delta\omega(t)$ undergoing a *discrete* SFM process that realises the only two discrete frequencies, $\omega_0 \pm \omega_\delta$, with equal probabilities.[17] Although this model is in principle available for the case of unequal probabilities,[59] but we reasonably employed the "equal" *discrete* SFM process in this study (see the ESI). Expanding this system to an N-independent two-state jump Markov process, in which the fluctuating frequency takes discrete values such as $\delta\omega = \pm\omega_\delta, \pm\sqrt{2}\omega_\delta, \ldots, \pm\sqrt{N}\omega_\delta$ (N: integer), the amplitude of random modulation is associated with the fluctuating frequency of the thermal bath as ${\omega_\Delta}^2 = N{\omega_\delta}^2$.[16] In this case, the complex susceptibility of the *discrete* SFM model, $\tilde{\chi}_{\mathrm{dSFM}}(\omega)$, is given by[16]

$$\tilde{\chi}_{\mathrm{dSFM}}(\omega) = \Delta\chi \left\{ 1 - i\omega \cfrac{1}{i(\omega-\omega_0) + \cfrac{N{\omega_\delta}^2}{i(\omega-\omega_0) + \Gamma + \cfrac{2(N-1){\omega_\delta}^2}{i(\omega-\omega_0) + 2\Gamma + \cdots \cfrac{N{\omega_\delta}^2}{i(\omega-\omega_0) + N\Gamma}}}} \right\} \quad (2)$$

where $\Delta\chi$ is the strength of the susceptibility. Since the SFM model is a generalized formula of the complex susceptibility reflecting stochastic modulation from the environment, it can deal with a relaxational band shape, by setting $\omega_0 = 0$:[20,21] for instance, the fast modulation limit $\alpha_{\mathrm{K}} \to 0$ coincides with the Debye function at any N. Similarly, the relaxation-type discrete SFM model is hardly dependent on N under the condition of $\alpha_{\mathrm{K}} \ll 1$ (see Fig. S3 of the ESI).[16] Hence, a relaxa-

193 tion line shape bearing a similarity to the Debye model, like the dielectric relaxation of water, can
194 be approximated by substituting $N = 1$ and $\omega_0 = 0$ into eqn (2):

$$\tilde{\chi}_{\mathrm{dSFM}}(\omega) = \frac{\Delta\chi {\omega_\delta}^2}{{\omega_\delta}^2 - \omega^2 + i\omega\Gamma} \tag{3}$$

195 The case of $\alpha_{\mathrm{K}} \ll 1$ eqn (3) is equivalent to the Rocard equation:[60,61] thus, our *discrete* SFM re-
196 laxation model includes the Debye (negligible inertia and non-interacting, namely, $\omega_\delta \to 0$ and
197 $1/\Gamma \to 0$) and the Rocard (non-interacting, $1/\Gamma \ll 1$) models as special cases.

198 In regard to the resonant case $\omega_0 \neq 0$, the SFM model should reproduce the inhomogeneous line
199 shapes of water libration.[62] In spite of this, the number of the *discrete* SFM processes ($= N$) of li-
200 bration cannot be determined from only the experimental results. To resolve this issue, we alterna-
201 tively fitted the libration bands with a *continuous* SFM model, in which the frequency fluctuation
202 $\delta\omega(t)$ follows a Gaussian probability distribution such that the instantaneous frequency $\omega(t)$ can
203 take continuous values.[17] Defining the standard deviation of the $\delta\omega(t)$ distribution as the ampli-
204 tude of stochastic modulation (ω_Δ), its complex susceptibility, $\tilde{\chi}_{\mathrm{cSFM}}(\omega)$, is given by[21]

$$\tilde{\chi}_{\mathrm{cSFM}}(\omega) = \Delta\chi \left\{ 1 - i\omega \frac{1}{i(\omega - \omega_0) + \dfrac{{\omega_\Delta}^2}{i(\omega - \omega_0) + \Gamma + \dfrac{2{\omega_\Delta}^2}{i(\omega - \omega_0) + 2\Gamma + \cdots}}} \right\} \tag{4}$$

205 The mathematical derivation and examples of the SFM model are shown in the ESI.

206 Because of the failure of the Debye relaxation model and incompatibility of the libration line
207 shape with the DHO model, we modified eqn (1) by applying the SFM model instead of them:

$$\tilde{\varepsilon}(\omega) = \tilde{\chi}_{\mathrm{slow}}(\omega) + \tilde{\chi}_{\mathrm{fast}}(\omega) + \tilde{\chi}_{\mathrm{B}}(\omega) + \tilde{\chi}_{\mathrm{S}}(\omega) + \tilde{\chi}_{\mathrm{L1}}(\omega) + \tilde{\chi}_{\mathrm{L2}}(\omega) + \varepsilon_{\infty}$$

$$= \frac{\Delta\varepsilon_{\mathrm{slow}}{\omega_{\delta}^{\mathrm{slow}}}^{2}}{{\omega_{\delta}^{\mathrm{slow}}}^{2} - \omega^{2} + i\omega\Gamma_{\mathrm{slow}}} + \frac{\Delta\varepsilon_{\mathrm{fast}}{\omega_{\delta}^{\mathrm{fast}}}^{2}}{{\omega_{\delta}^{\mathrm{fast}}}^{2} - \omega^{2} + i\omega\Gamma_{\mathrm{fast}}} + \frac{\Delta V_{\mathrm{B}}{\omega_{\mathrm{B}}}^{2}}{{\omega_{\mathrm{B}}}^{2} - \omega^{2} + i\omega\gamma_{\mathrm{B}}} + \frac{\Delta V_{\mathrm{S}}{\omega_{\mathrm{S}}}^{2}}{{\omega_{\mathrm{S}}}^{2} - \omega^{2} + i\omega\gamma_{\mathrm{S}}}$$

$$+\Delta V_{\mathrm{L1}}\left\{1 - i\omega\frac{1}{i(\omega-\omega_{\mathrm{L1}}) + \dfrac{{\omega_{\Delta}^{\mathrm{L1}}}^{2}}{i(\omega-\omega_{\mathrm{L1}}) + \Gamma_{\mathrm{L1}} + \dfrac{2{\omega_{\Delta}^{\mathrm{L1}}}^{2}}{i(\omega-\omega_{\mathrm{L1}}) + 2\Gamma_{\mathrm{L1}} + \cdots}}}\right\}$$

$$+\Delta V_{\mathrm{L2}}\left\{1 - i\omega\frac{1}{i(\omega-\omega_{\mathrm{L2}}) + \dfrac{{\omega_{\Delta}^{\mathrm{L2}}}^{2}}{i(\omega-\omega_{\mathrm{L2}}) + \Gamma_{\mathrm{L2}} + \dfrac{2{\omega_{\Delta}^{\mathrm{L2}}}^{2}}{i(\omega-\omega_{\mathrm{L2}}) + 2\Gamma_{\mathrm{L2}} + \cdots}}}\right\} + \varepsilon_{\infty} \qquad (5)$$

where, $\omega_{\delta}^{\mathrm{slow(fast)}}$ is the modulation amplitude and $\Gamma_{\mathrm{slow(fast)}}$ is the modulation frequency of the *discrete* SFM relaxation processes, and $\omega_{\Delta}^{\mathrm{L1(L2)}}$ is the modulation amplitude and $\Gamma_{\mathrm{L1(L2)}}$ is the modulation frequency of the *continuous* SFM resonant processes. The other parameters are identical to eqn (1). For successful fits, the parameter γ_{B} of D_2O was fixed to be the same as that of H_2O, in reference to the small isotopic dependence of γ_{B}.[20,30] Moreover, $\Gamma_{\mathrm{L1(L2)}}/2\pi$ was also constrained to be 1.4 THz by reference to the librational correlation time of 115 fs.[63] Fig. 3(a)(b) shows that the resulting complex susceptibilities fitted with eqn (5) well replicate the experimental $\tilde{\varepsilon}(\omega)$. As can be seen in Fig. 3(c), after subtracting the overwhelming contribution of the slow relaxation, the fitted results are in quite good agreement with the "residual" complex dielectric constant: this result highlights the excellence of the SFM fitting of eqn (5). The best-fitted parameters are summarized in Table 1 and 2.

Consistency of the SFM relaxation modes with the experimental results. As depicted in Fig. 3, $\tilde{\chi}_{\mathrm{slow}}(\omega)$ and $\tilde{\chi}_{\mathrm{fast}}(\omega)$ reproduced by eqn (5) exhibit similar shapes to those of the Debye model below 1 THz, owing to a small α_{K} (Table 1). The result indicates that the modulation degree is very modest in the dielectric spectrum, in stark contrast with the depolarized low-frequency Raman spectrum in which a Raman-active relaxation around 200 GHz for H_2O is strongly modulated ($\alpha_{\mathrm{K}} \approx 0.7$ at 300 K, note that the Raman-active relaxation frequency is close to that of our $\tilde{\chi}_{\mathrm{fast}}(\omega)$).[20,24] This discrepancy may point to different water relaxation dynamics (i.e. vectorial and tensorial characters of the responses) probed by dielectric and Raman spectroscopy.[32]

It deserves special emphasis that the high-frequency tail of the SFM relaxation modes starts to fall more sharply in the THz region, for $\alpha_{\mathrm{K}} \neq 0$. This is because our SFM model assuming a coupling with an oscillatory fluctuation of the thermal bath leads to a rapid decrease at a rate proportional to ω^{-3} far above the relaxation frequency, while the Debye model decays as ω^{-1}. Fig. 4 clearly shows that the SFM model is consistent with the experimental imaginary part up to 400 THz, as opposed to the Debye model and defect-migration theory that obviously exceed the experimental result above 60 THz. From this result, it is evident that the SFM model reconciles the failure of the Debye one. Given that the SFM model starts to deviate from the Debye model around 3 THz, the intermolecular modes in the THz region are supposed to be more precisely extracted by the SFM model.

We also obtained the response function of the relaxations $\chi_{\mathrm{relax}}(t)$ to examine the model dependence in the time-domain. As shown in Fig. 5(a), the deviation of the Debye model in the high frequency tail is reflected in the inertial non-exponential behaviour at the very onset of the decay followed by the perfectly exponential long-term behaviour (see the inset). Meanwhile, the Debye relaxation applies a long-time approximation even to $t \to 0$, and it doesn't incorporate the short-time behaviour of the relaxing dipoles.[10,11] Taking into account that the inertial effect of the relaxing dipoles is not cancelled out at short times,[10] the main reason for the initial curvature of the SFM response function can be traced to the molecular moment of inertia (i.e. finite ω_δ). As for the slow relaxation, it is intriguing that $\omega_\delta^{\mathrm{slow}}/2\pi \approx 0.3$ THz and $\omega_\delta^{\mathrm{fast}}/2\pi \approx 1.5$ THz for both H_2O and D_2O obtained in our fitting coincides with the frequency range dominated by the relaxation and the intermolecular vibrations (see Fig. 3). This accordance implies that these HB dynamics of water may hinder buildup of torques of the relaxation motion. Nevertheless, the very short correlation time of the thermal bath, $\Gamma_{\mathrm{slow}}{}^{-1} \approx \Gamma_{\mathrm{fast}}{}^{-1} \approx 25$ fs obtained in this study, in good agreement with an earlier prediction (28 fs, at 295 K) [64], indicates that the effect of inertia persists only temporarily, presumably due to the ultrafast memory loss of correlations in the HB structure.[51] After the correlation is lost, the relaxing dipoles start to behave statistically, turning the initial non-exponential decay into an exponential one (Fig. 5(a)).

The best-fitted parameters in Table 1 show that the relaxation time is almost model-independent

for both H_2O and D_2O. On the other hand, compared with the Debye model, the SFM model slightly underestimated the relaxation strengths $\Delta\varepsilon_{\mathrm{slow}}$ and $\Delta\varepsilon_{\mathrm{fast}}$ because the marginally decreased response function at short times diminishes the time-averaged effective dipole moment. These short-time dynamics, however, have a negligible effect on the relaxation time τ as it mainly depends on the long-time behaviour.

Refined band shapes of the intermolecular vibrations. As shown in Fig. 3 and Fig. S4 of the ESI, the libration band of liquid water is more accurately reproduced by the resonance-type SFM model than by the dual-DHO one. The existence of the two sub-bands points to different librational dynamics reflecting the anisotropic moment of inertia of a water molecule: along the out-of-plane direction (*x*-axis: see Fig. S4 of the ESI), along the in-plane direction perpendicular to the dipole vector (*y*-axis) and along the dipole vector direction (*z*-axis).[65-67] MD simulation studies showed that the *x*- and *z*-axis components of liquid H_2O give rise to indistinguishable symmetric peaks in the rotational vibration density of states (VDOS) spectra around 15 THz and the *y*-axis counterpart yields a distinctive peak in the higher frequency.[65-67] Among them, the *z*-axis component is IR-inactive because there are small dipole moment changes induced by the rotation. The two sub-bands obtained in our SFM fitting are close in frequency to the *x*- and *y*-axis libration components in the VDOS spectra,[65-67] which suggests that the present L1 and L2 components are due to the hindered rotations along the out-of-plane (*x*-axis) and the perpendicular to the dipole vector

(y-axis) directions, respectively.

In eqn (5), we modelled the libration bands as two *continuous* SFM processes, assuming a Gaussian probability distribution of the fluctuating frequency $\delta\omega(t)$ under the correlation time with the thermal bath of $\Gamma_{\mathrm{L}}^{-1} = 115$ fs. Our SFM fitting ends up showing that each libration sub-band moderately undergoes slow modulation ($\alpha_{\mathrm{K}} \approx 3.0$), when compared with the fast modulation character of the hindered translation modes (as described later). For the L1 and L2 modes, the amplitude of the stochastic modulation is found to be $\omega_{\Delta}/2\pi \approx 4.2$ THz: this indicates the water modes below 4.2 THz, as represented by the hindered translations, play a crucial role in the slow modulation of the libration band.[68] This scenario accords with previous computational studies, which demonstrated that large anharmonicity of the libration mode leads to strong coupling with the hindered translation dynamics.[63,69] Moreover, the reported correlation time of libration inhomogeneity (as long as 105~115 fs)[63,70] coincides with the excitation period of the intermolecular bending and stretching motions (typically 100 fs, as shown in Fig. 5(b)), providing qualitative insight into the coupling between the libration and translation modes. Hence, disturbance of the HB structure caused by the hindered translations leads to slow modulation of the libration band. It is clear from the time-domain function in Fig. 5(b) that slow modulation of the libration modes is rather pronounced as an inertial behaviour at short times, in contrast to the sharp decay observed in the DHO models.

As shown in Table 2, when the relaxation and libration modes are reproduced by the SFM model, the best-fitted intermolecular stretching DHO parameters (ΔV_S, ω_S and γ_S) become larger whereas the bending parameters remain almost unchanged from those obtained by eqn (1). The primary reasons for this model dependence are that the SFM relaxations significantly fall below the Debye model's predictions above 3 THz, and the libration band formulated by the continuous SFM model is suppressed below 10 THz (see Fig. 3 and 4, in the imaginary part). These factors are compensated for by the increased contribution of the stretching mode (i.e. enhancing ΔV_S, up-shifting ω_S, and broadening γ_S), while they have little influence on the complex dielectric constant around 1.5 THz where the bending vibration is located. See the ESI for a more detailed discussion on the hindered translation modes.

Finally, we would like to comment on why these hindered translation modes can be approximated by the fast modulation (=homogeneous) DHO function, contrary to the slow modulation (=inhomogeneous) origin of the libration modes. As stated earlier, the slow modulation line shape is achieved when the modulation degree α_K is high: more specifically, when the modulation rate is adequately smaller than the resonant frequency $\omega_0 \gg \Gamma$.[71] Yet, a previous computational study has shown that the frequency correlation of the hindered translation motion is very rapidly lost (< 20 fs, corresponding to $\Gamma > 50$ THz).[63,72] From this perspective, the resonant frequencies of the hindered translation modes are so small that their line shapes remain fast modulation because of the insuffi-

cient interaction time with the thermal bath.

4. Conclusions

In order to reexamine the relaxational and vibrational line shapes of liquid H_2O and D_2O, the complete dielectric constants from 500 MHz to 400 THz were measured. In the framework of the conventional Debye-DHO fitting, the Debye model fails above the IR region, and the DHO model does not accurately reproduce the libration band. We overcame these limitations by applying the SFM model assuming a frequency modulation through the correlation with the thermal bath. Unlike the Debye model, our SFM relaxation model was consistent with the experimental dielectric spectra up to 400 THz on account of small but non-negligible correlations with the HB dynamics. In regard to the time-domain response functions, the failure of the Debye model can be traced to its completely exponential behaviour, whereas our SFM model clearly shows that the moment of inertia hinders the water reorientation with a persistence time of typically 25 fs. By applying the SFM model to the libration mode, we showed that it consists of two sub-bands reflecting different rotational axes. It is striking that the libration sub-bands undergo slow modulation through the hindered translation modes. It follows that disturbance of the water HBs owing to the hindered translations cause frequency fluctuations and eventually yield slow modulation of the libration band. On the other hand, the hindered translation modes such as the intermolecular bending and stretching were closely approximated by the homogeneous DHO functions, probably because fluctuations associated with the

HB dynamics are so fast that their line shapes remain fast modulation.

Although the large relaxation mode of liquid water around 20 GHz has gained much attention from researchers interested in studying dielectric relaxation, it is merely regarded as the absorption baseline by researchers studying vibration spectroscopy. Our ultrabroadband spectroscopy unifies these independently discussed research areas, revealing the limitation of the phenomenologically accepted Debye model. More importantly, our SFM model can be a means by which we can arrive at a more accurate understanding of the water relaxation and vibration dynamics. Accordingly, this approach may be also helpful in describing interfacial water and biological water.

Conflicts of interest

There are no conflicts to declare.

Acknowledgements

We thank Mr. Masahito Nakamura, Dr. Katsuhiro Ajito and Dr. Takuro Tajima (NTT Corporation, Japan) for providing the experimental data in the microwave region. The continued support during experiments of Professor Shojiro Kikuchi (Hyogo College of Medicine, Japan) and Dr. Naotaka Yoshikawa (University of Tokyo, Japan) are also greatly appreciated. Financial support was provided by Grants-in-Aid for JSPS Research Fellows Grant Number 26295, Industry-Academia Collaborative R&D from JST, RIKEN Special Postdoctoral Researcher Program and RIKEN Incentive Research Projects.

References

(1) U. Kaatze, *J. Chem. Eng. Data*, 1989, **34**, 371.

(2) R. Buchner, J. Barthel and J. Stauber, *Chem. Phys. Lett.*, 1999, **306**, 57.

(3) D. C. Elton, *Phys. Chem. Chem. Phys.*, 2017, **19**, 18739.

(4) C. Rønne, L. Thrane, P.-O. Åstrand, A. Wallqvist, K. V. Mikkelsen and S. R. Keiding, *J. Chem. Phys.*, 1997, **107**, 5319.

(5) H. Yada, M. Nagai and K. Tanaka, *Chem. Phys. Lett.*, 2008, **464**, 166.

(6) A. Y. Zasetsky, *Phys. Rev. Lett.*, 2011, **107**, 117601.

(7) A. Beneduci. *J. Mol. Liq.*, 2008, **138**, 55.

(8) I. Popov, P. B. Ishai, A. Khamzin and Y. Feldman, *Phys. Chem. Chem. Phys.*, 2016, **18**, 13941.

(9) N. Bjerrum, *Science*, 1952, **115**, 385.

(10) J. P. Hansen, D. Levesque and J. Zinn-Justin, *Liquids, Freezing and the Glass Transition*, North-Holland, Netherlands, 1991.

(11) R. G. Gordon, *J. Chem. Phys.*, 1965, **43**, 1307.

(12) D. McMorrw and W. T. Lotshaw, *J. Phys. Chem.*, 1991, **95**, 10395.

(13) J. T. Kindt and C. A. Schmuttenmaer, *J. Phys. Chem.*, 1996, **100**, 10373.

(14) G. M. Hale and M. R. Querry, *Appl. Opt.*, 1973, **12**, 555.

(15) H. D. Downing and D. Williams, *J. Geophys. Res.*, 1975, **80**, 1656.

(16) F. Shibata, C. Uchiyama and K. Maruyama, *Physica A*, 1989, **161**, 42.

(17) R. Kubo, in Stochastic Processes in Chemical Physics, ed. K. E. Shuler, Wiley, London, 1969, 6, 101.

(18) Y. Amo and Y. Tominaga, *Phys. Rev. E*, 1999, **60**, 1708.

(19) G. E. Walrafen, *J. Chem. Phys.*, 1967, **47**, 114.

(20) Y. Amo and Y. Tominaga, *Physica A*, 2000, **276**, 401

(21) K. Winkler, J. Lindner and P. Vöhringer, *Phys. Chem. Chem. Phys.*, 2002, **4**, 2144.

(22) H. Yada, M. Nagai and K. Tanaka, *Chem. Phys. Lett.*, 2009, **473**, 279.

(23) A. Taschin, P. Bartolini, R. Eramo, R. Righini and R. Torre, *Nat. Commun.*, 2013, **4**, 2401.

(24) T. Fukasawa, T. Sato, J. Watanabe, Y. Hama, W. Kunz and R. Buchner, *Phys. Rev. Lett.*, 2005, **95**, 197802.

(25) M. Nagai, H. Yada, T. Arikawa and K. Tanaka, *Int. J. Infrared Milli. Wave*s, 2006, **27**, 505.

(26) K. Shiraga, Y. Ogawa, K. Tanaka, T. Arikawa, N. Yoshikawa, M. Nakamura, K. Ajito and T.

Tajima, *J. Phys. Chem. B*, 2018, **122**, 1268.

(27) J. E. Bertie and Z. Lan, *J. Chem. Phys.*, 1996, **105**, 8502.

(28) K. Shiraga, T. Suzuki, N. Kondo and Y. Ogawa, *J. Chem. Phys.*, 2014, **141**, 235103.

(29) K. Shiraga, A. Adachi and Y. Ogawa, *Chem. Phys. Lett.*, 2017, **678**, 59.

(30) H. R. Zelsmann, *J. Mol. Struc.*, 1995, **350**, 95.

(31) T. Wang, P. Klarskov and P. U. Jepsen, *IEEE Trans. Terahertz Sci. Technol.*, 2014, **4**, 425.

(32) J. S. Hansen, A. Kisliuk, A. P. Sokolov and C. Gainaru, *Phys. Rev. Lett.*, 2016, **116**, 237601.

(33) P. Lunkenheimer, S. Emmert, R. Gulich, M. Kohler, M. Wolf, M. Schwab and A. Loidl, *Phys. Rev. E*, 2017, **96**, 062607.

(34) C. Rønne, P.-O. Åstrand and S. R. Keiding, *Phys. Rev. Lett.*, 1999, **82**, 2888.

(35) M. Sharma, R. Resta and R. Car, *Phys. Rev. Lett.*, 2005, **95**, 187401.

(36) M. Heyden, J. Sun, S. Funkner, G. Mathias, H. Forbert, M. Havenith and D. Marx, *Proc. Natl. Acad. Sci. USA*, 2010, **107**, 12068.

(37) H. Torii, *J. Phys. Chem. B*, 2011, **115**, 6636.

(38) E. Guardia, I. Skarmoutsos and M. Masia, *J. Phys. Chem. B*, 2014, **119**, 8926.

(39) C. Rønne and S. R. Keiding, *J. Mol. Liq.*, 2002, **101**, 199.

(40) U. Balucani, J. P. Brodholt and R. Vallauri, *J. Phys.: Condens. Matter*, 1996, **8**, 9269.

(41) G. Sutmann and R. Vallauri, *J. Phys.: Condens. Matter*, 1998, **10**, 9231.

(42) G. Garberoglio, R. Vallauri and G. Sutmann, *J. Chem. Phys.*, 2002, **117**, 3278.

(43) A. De Santis, A. Ercoli and D. Rocca, *Phys. Rev. Lett.*, 1999, **82**, 3452.

(44) A. De Santis, A. Ercoli and D. Rocca, *J. Chem. Phys.*, 2004, **120**, 1657.

(45) K. H. Tsai and T.-M. Wu, *Chem. Phys. Lett.*, 2006, **417**, 389.

(46) D. Laage, G. Stirnemann, F. Sterpone, R. Rey and J. T. Hynes, *Annu. Rev. Phys. Chem.*, 2011, **62**, 395.

(47) Y. Maréchal, *J. Chem. Phys.*, 1991, **95**, 5565.

(48) J.-B. Brubach, A. Mermet, A. Filabozzi, A. Gerschel and P. Roy, *J. Chem. Phys.*, 2005, **122**, 184509.

(49) C. P. Lawrence and J. L. Skinner, *J. Chem. Phys.*, 2003, **118**, 264.

(50) J. D. Eaves, J. J. Loparo, C. J. Fecko, S. T. Roberts, A. Tokmakoff and P. L. Geissler, *Proc. Natl. Acad. Sci. USA*, 2005, **102**, 13019.

(51) M. L. Cowan, B. D. Bruner, N. Huse, J. R. Dwyer, B. Chugh, E. T. J. Nibbering, T. Elsaesser

and R. J. D. Miller, *Nature*, 2005, **434**, 199.

(52) D. Kraemer, M. L. Cowan, A. Paarmann, N. Huse, E. T. J. Nibbering, T. Elsaesser and R. J. Dwayne Miller, *Proc. Natl. Acad. Sci. USA*, 2008, **105**, 437.

(53) C. H. Collie, J. B. Hasted and D. M. Ritson, *Proc. Phys. Soc.*, 1948, **60**, 145.

(54) U. Kaatze, *Chem. Phys. Lett.*, 1993, **203**, 1.

(55) G. A. Vidulich, D. F. Evans, R. L. Kay, *J. Phys. Chem.*, 1966, **71**, 656.

(56) J. L. Doob, *Stochastic Processes*, Wiley, New York, 1953.

(57) J. R. Schmidt, N. Sundlass and J. L. Skinner, *Chem. Phys. Lett.*, 2003, **378**, 559.

(58) C. Uchiyama and F. Shibata, *Physica A*, 1988, **153**, 469.

(59) Y. Amo, Y. Kameda and T. Usuki, *AIP Adv.*, 2016, **6**, 055319.

(60) M. Y. Rocard, *J. Phys. Radium*, 1933, **4**, 247.

(61) W. T. Coffey, Y. P. Kalmykov and S. V. Titov, *Phys. Rev. E*, 2002, **65**, 032102.

(62) J. G. Saven and J. L. Skinner, *J. Chem. Phys.*, 1993, **99**, 4391.

(63) T. Yagasaki and S. Saito, *J. Chem. Phys.*, 2008, **128**, 154521.

(64) K. F. Herzfeld, *J. Am. Chem. Soc.*, 1964, **86**, 3468.

(65) M. Cho, G. R. Fleming, S. Saito, I. Ohmine and R. M. Stratt, *J. Chem. Phys.*, 1994, **100**, 6672.

(66) S. L. Chang, T.-M. Wu and C-Y. Mou, *J. Chem. Phys.*, 2004, **121**, 3605.

(67) M. T. Sonoda, N. H. Moreira, L. Martínez, F. W. Favero, S. M. Vechi, L. R. Martins and M. S. Skaf, *Braz. J. Phys.*, 2004, **34**, 3.

(68) T. Yagasaki and S. Saito, *J. Chem. Phys.*, 2011, **134**, 184503.

(69) M. Demirplak and S. A. Rice, *J. Chem. Phys.*, 2002, **116**, 8028.

(70) S. Saito and I. Ohmine, *J. Chem. Phys.*, 2006, **125**, 084506.

(71) T. Ikeda, H. Ito and Y. Tanimura, *J. Chem. Phys.*, 2015, **142**, 212421.

(72) B. J. Loughnane, A. Scodinu, R. A. Farrer, J. T. Fourkas and U. Mohanty, *J. Chem. Phys.*, 1999, **111**, 2686.

(73) H. Ito and Y. Tanimura, *J. Chem. Phys.*, 2016, **144**, 074201.

Table 1 Best-fitted relaxation parameters of Debye and discrete SFM model for liquid H_2O and D_2O at 300 K. Uncertainties are shown in parentheses.

	Debye model, eqn (1)				Discrete SFM model, eqn (5)					
	$\Delta\varepsilon_{\mathrm{slow}}$ (-)	τ_{slow} (ps)	$\Delta\varepsilon_{\mathrm{fast}}$ (-)	τ_{fast} (ps)	$\Delta\varepsilon_{\mathrm{slow}}$ (-)	τ_{slow} (ps)	$\alpha_{\mathrm{K(slow)}}$ (-)	$\Delta\varepsilon_{\mathrm{fast}}$ (-)	τ_{fast} (ps)	$\alpha_{\mathrm{K(fast)}}$ (-)
H_2O	71.82	7.96	1.66	0.53	71.64	7.98	0.05	1.59	0.53	0.21
	(0.01)	(0.01)	(0.03)	(0.01)	(0.02)	(0.01)	(0.01)	(0.04)	(0.03)	(0.04)
D_2O	71.74	9.90	1.67	0.64	71.56	9.92	0.05	1.60	0.64	0.20
	(0.01)	(0.01)	(0.02)	(0.01)	(0.01)	(0.01)	(0.01)	(0.02)	(0.02)	(0.03)

Table 2 Best-fitted DHO parameters of eqn (1) and eqn (5) for liquid H_2O and D_2O at 300 K. Uncertainties are shown in parentheses.

	Eqn (1)						Eqn (5)					
	ΔV_{B} (-)	$\omega_{\mathrm{B}}/2\pi$ (THz)	$\gamma_{\mathrm{B}}/2\pi$ (THz)	ΔV_{S} (-)	$\omega_{\mathrm{S}}/2\pi$ (THz)	$\gamma_{\mathrm{S}}/2\pi$ (THz)	ΔV_{B} (-)	$\omega_{\mathrm{B}}/2\pi$ (THz)	$\gamma_{\mathrm{B}}/2\pi$ (THz)	ΔV_{S} (-)	$\omega_{\mathrm{S}}/2\pi$ (THz)	$\gamma_{\mathrm{S}}/2\pi$ (THz)
H_2O	0.32	1.45	1.59	1.29	5.12	5.42	0.30	1.34	1.58	1.68	5.33	6.51
	(0.03)	(0.03)	(0.13)	(0.01)	(0.02)	(0.07)	(0.10)	(0.01)	(0.40)	(0.02)	(0.02)	(0.10)
D_2O	0.39	1.40	1.59*	1.13	5.10	5.19	0.35	1.33	1.58*	1.47	5.23	5.83
	(0.02)	(0.02)		(0.09)	(0.07)	(0.20)	(0.02)	(0.02)		(0.04)	(0.02)	(0.17)

* Fixed.

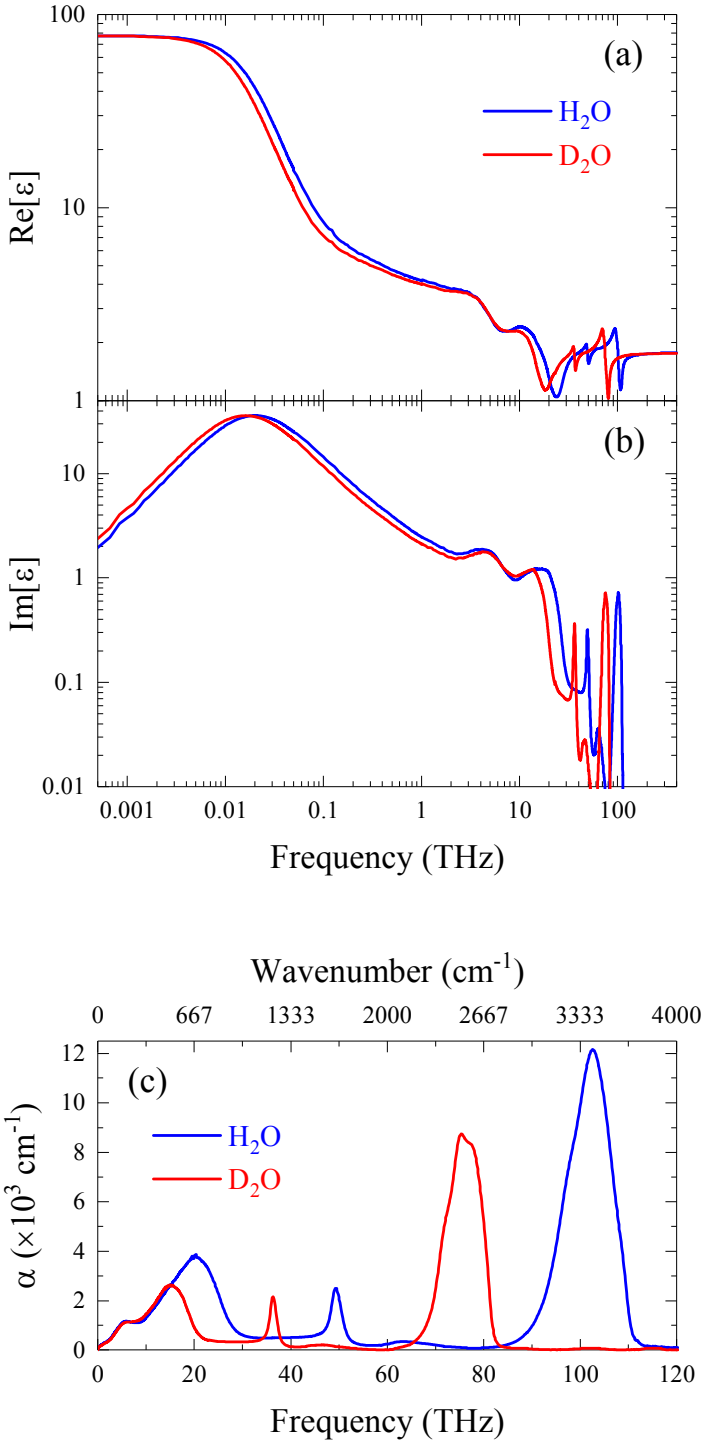

Fig. 1 (a,b) Ultrabroadband complex dielectric constant (500 MHz ~ 400 THz) of liquid H_2O and D_2O at 300 K. (c) Absorption coefficient of H_2O and D_2O at 300 K up to 120 THz, determined from the complex dielectric constant.

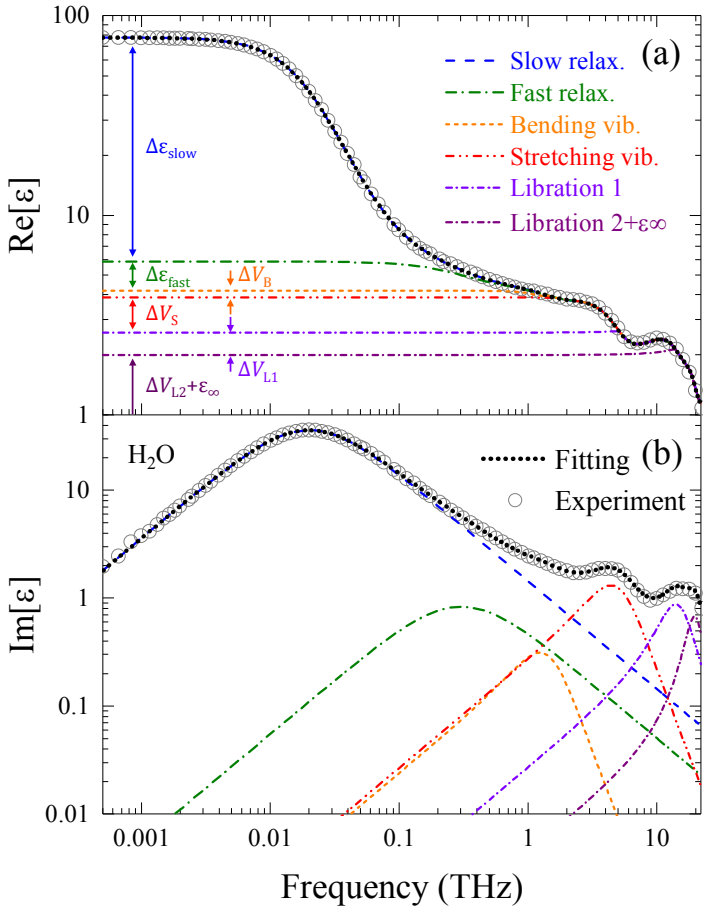

Fig. 2 Debye-DHO fitting of the complex dielectric constant of H_2O (500 MHz ~ 23 THz) described by eqn (1). The experimental result (gray open circles) is reproduced by the fitting curve, which consists of two Debye- and four DHO-type susceptibilities.

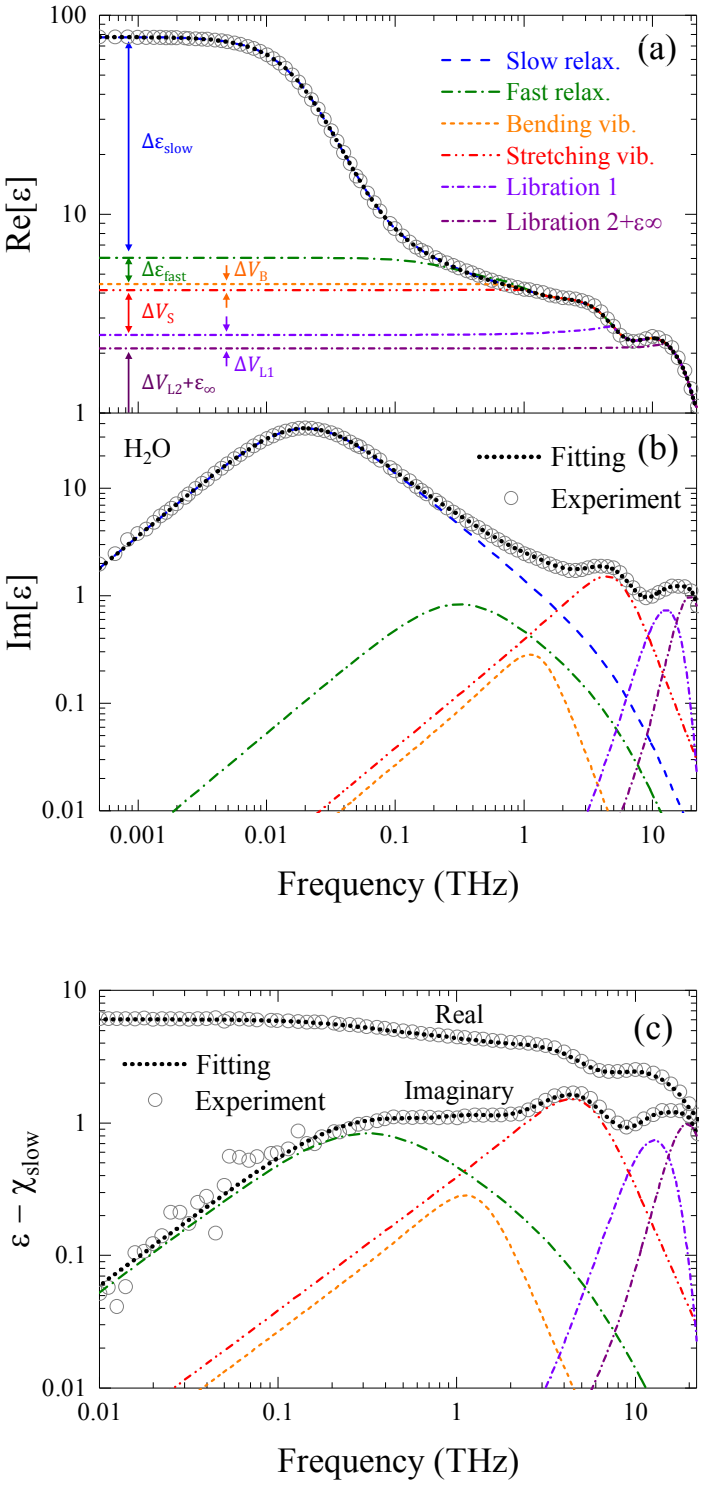

Fig. 3 (a,b) SFM fitting of the complex dielectric constant of H_2O (500 MHz ~ 23 THz), described by eqn (5). The experimental result (gray open circles) is reproduced by the fitting curve, which consists of two relaxation-type discrete SFM, two DHO, and two resonance-type continuous SFM susceptibilities. (c) Residual complex dielectric constant of H_2O determined by subtracting the contribution of the slow relaxation process from the experimental result.

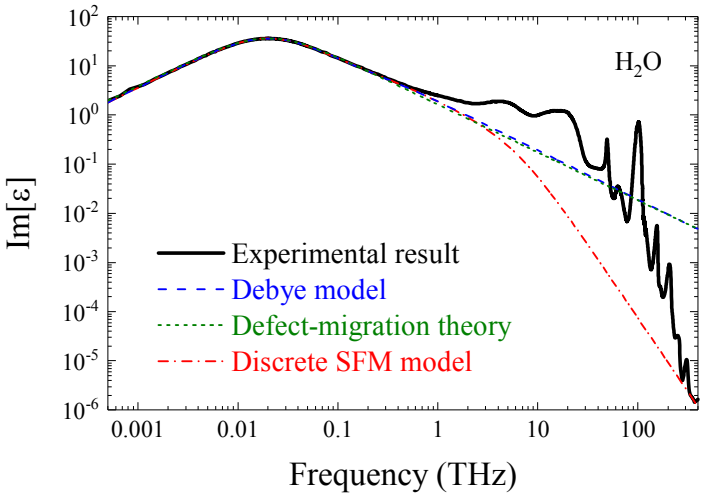

Fig. 4 Experimental imaginary part of H_2O compared with its constituent relaxation mode described by the Debye model, the defect-migration theory,[8] and the discrete SFM model. Note that the Debye and discrete SFM model include both the slow and fast relaxation processes. The shaded area, $\mathrm{Im}[\tilde{\varepsilon}(\omega) - \tilde{\chi}_{\mathrm{dSFM}}(\omega)]$, corresponds to the contribution of the vibration modes of water. It can be seen that the contribution of the SFM relaxations sufficiently falls below the actual imaginary part in the IR region, which ensures that the relaxations can be regarded as the absorption background.

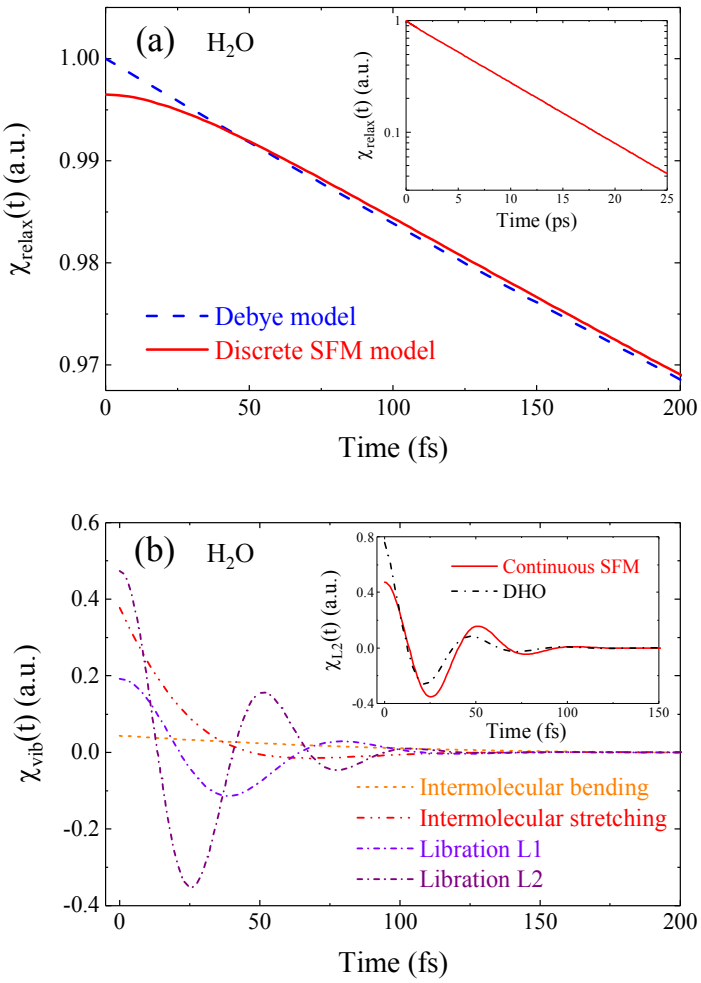

Fig. 5 (a) Response function $\chi_{\text{relax}}(t) = \mathcal{F}^{-1}[\tilde{\chi}_{\text{slow}}(\omega) + \tilde{\chi}_{\text{fast}}(\omega)]$ of H_2O described by the Debye and discrete SFM model. The vertical axis is normalized so that the Debye model satisfies $\chi_{\text{relax}}(0) = 1$. The inset is a semi-logarithmic plot of the discrete SFM model up to 25 ps. (b) Time-domain functions $\chi_{\text{vib}}(t)$ of the intermolecular bending (dashed line), intermolecular stretching (two-dot-dashed), and two libration modes (dot-dashed) of H_2O. Note that the bending signal is amplified by a factor of 10 for clarity. The inset shows the comparison of the L2 response function expressed by the continuous SFM (eqn (5)) and DHO (eqn (1)) functions, revealing the inertial behaviour at short times.

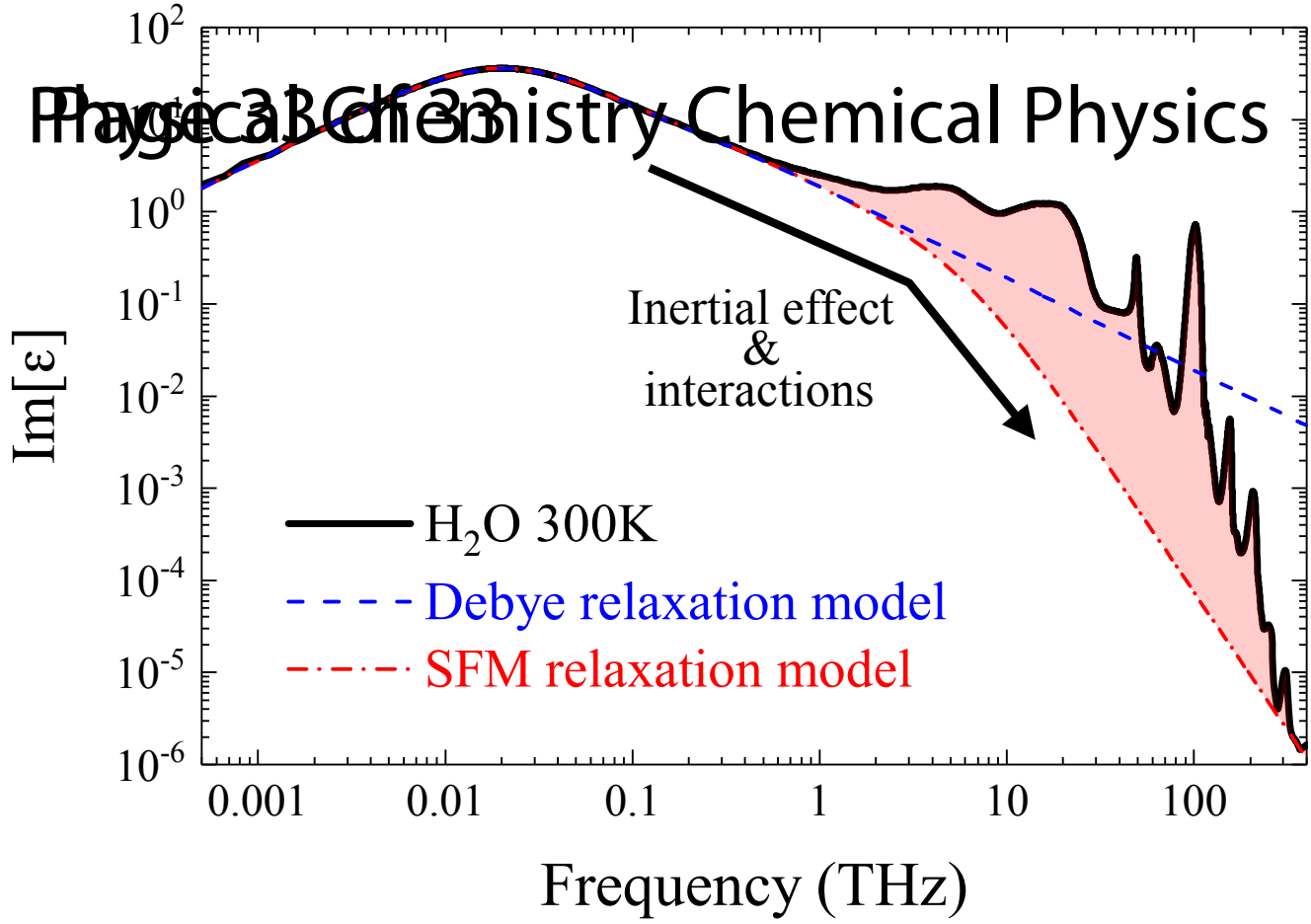
Im[ε]
Frequency (THz)
Inertial effect
&
interactions
H2O 300K
Debye relaxation model
SFM relaxation model